

Dynamic Origin of Long-Range Concentration Correlations in Nonequilibrium Diffusion: A Computational Fluctuating Hydrodynamics Approach

Anonymous Author(s)

Anonymous Institution

ABSTRACT

Nonequilibrium diffusive systems driven by macroscopic concentration gradients exhibit anomalous long-range correlations in concentration fluctuations, characterized by a structure factor scaling as $S(q) \sim q^{-4}$. While the steady-state form is well established through fluctuating hydrodynamics (FHD), the *dynamical mechanism* by which these correlations emerge from an initially uncorrelated state remains an open problem in nonequilibrium statistical mechanics. We address this problem through a combined analytical and computational approach. We derive the transient structure factor $S_{\text{neq}}(q, t) = S_{\text{neq}}^{\text{ss}}(q) [1 - \exp(-2\Gamma(q)t)]$ from the linearized FHD equations for a binary mixture under a suddenly imposed gradient, where $\Gamma(q)$ is a q -dependent relaxation rate encoding the coupled concentration-velocity dynamics. We validate this prediction using stochastic partial differential equation (SPDE) simulations of the coupled system on a 128×128 lattice. Our key findings are: (i) correlations build up *hierarchically*, with short-wavelength modes equilibrating on diffusive timescales $\sim 1/(Dq^2)$ before long-wavelength modes; (ii) the correlation length grows as $\xi(t) \sim \sqrt{Dt}$ at early times, saturating at the gravity-determined scale $1/q_c$; (iii) the transient exhibits dynamical scaling collapse $S_{\text{neq}}(q, t)/S_{\text{neq}}^{\text{ss}}(q) = f(q^2Dt)$ with a universal function $f(x) = 1 - e^{-2x}$; and (iv) the fundamental mechanism is the time-dependent mode-coupling between concentration and velocity fluctuations mediated by the macroscopic gradient, which transfers the long-range character of hydrodynamic interactions into concentration correlations. These results provide a quantitative dynamical theory for the emergence of nonequilibrium long-range order in diffusive systems.

CCS CONCEPTS

- Computing methodologies → Modeling and simulation;
- Applied computing → Physical sciences and engineering.

KEYWORDS

nonequilibrium statistical mechanics, fluctuating hydrodynamics, long-range correlations, diffusion, stochastic PDE simulation

1 INTRODUCTION

When a macroscopic concentration gradient is imposed on a binary fluid mixture—for example, by maintaining different solute concentrations at opposing boundaries—the system is driven out of thermodynamic equilibrium. A striking consequence is the emergence of *giant fluctuations*: anomalously large, long-range correlations in the concentration field that have no equilibrium counterpart [18]. These correlations are characterized by a static structure factor that diverges as $S(q) \sim q^{-4}$ at small wavevectors q , indicating

power-law spatial correlations extending far beyond any molecular interaction range.

The steady-state properties of these nonequilibrium correlations are well understood within the framework of fluctuating hydrodynamics (FHD) [10, 14]. The linearized stochastic Navier-Stokes and diffusion equations predict the q^{-4} enhancement through the advective coupling between concentration and velocity fluctuations in the presence of the macroscopic gradient [13, 15]. Gravity provides a long-wavelength cutoff q_c below which buoyancy stabilizes the fluctuations [17]. Experimental confirmations are extensive, including shadowgraphy [3, 18], small-angle light scattering [1], and microgravity experiments [16].

However, a fundamental question remains open: *how do these long-range correlations dynamically emerge?* As highlighted by Maes [12] in a recent survey of open nonequilibrium problems, while the steady-state correlations are experimentally well established, the dynamical pathway by which they are generated from an initially uncorrelated state is not known. This is item 5 in Maes' list of open problems concerning the derivation of induced forces and interactions in nonequilibrium systems.

Understanding the dynamical origin is important for several reasons. First, it reveals the *mechanism* underlying the emergence of nonequilibrium order—the process, not just the endpoint. Second, it makes predictions about transient experiments where the gradient is suddenly imposed and the system relaxes toward the nonequilibrium steady state (NESS). Third, it establishes the hierarchy of timescales governing the approach to NESS, which is relevant for interpreting time-resolved scattering experiments [2, 4].

In this paper, we address this open problem through a combined analytical and computational approach. We solve the time-dependent linearized FHD equations for a binary mixture under a suddenly imposed concentration gradient, deriving an explicit formula for the transient structure factor $S_{\text{neq}}(q, t)$. We validate this prediction using stochastic PDE simulations of the coupled concentration-velocity system on a two-dimensional lattice.

Our main contributions are:

- (1) A closed-form analytical expression for $S_{\text{neq}}(q, t)$ that describes the complete transient from equilibrium to NESS, governed by a q -dependent relaxation rate $\Gamma(q)$.
- (2) Numerical verification through SPDE simulations of the linearized FHD system, demonstrating the hierarchical buildup of correlations and the evolution toward the q^{-4} scaling.
- (3) Identification of a dynamical scaling regime where $S_{\text{neq}}(q, t)/S_{\text{neq}}^{\text{ss}}(q)$ collapses onto a universal function of the scaling variable q^2Dt .

- 117 (4) Quantitative characterization of the growing correlation
 118 length $\xi(t) \sim \sqrt{Dt}$ that describes the progressive spatial
 119 extent of the emerging correlations.

120 1.1 Related Work

121 *Fluctuating Hydrodynamics.* The Landau-Lifshitz framework [10]
 122 and its extensions [8] provide the theoretical foundation for de-
 123 scribing thermal fluctuations in fluids. For binary mixtures, Ortiz
 124 de Zárate and Sengers [13, 14] derived the nonequilibrium enhance-
 125 ment of the structure factor in steady state, establishing the q^{-4}
 126 scaling law.

127 *Experimental Observations.* Giant fluctuations were first observed
 128 by Vailati and Giglio [18] using quantitative shadowgraphy. The
 129 gravitational cutoff was characterized by Vailati and Giglio [17].
 130 Microgravity experiments [16] confirmed the q^{-4} scaling over ex-
 131 tended ranges by removing the gravitational suppression. Croccolo
 132 et al. [3, 4] studied the dynamics of these fluctuations, providing
 133 some of the first time-resolved measurements.

134 *Computational Approaches.* Numerical methods for fluctuating
 135 hydrodynamics have been developed by Donev et al. [6] and Delong
 136 et al. [5], providing tools for simulating the stochastic PDEs govern-
 137 ing concentration and velocity fluctuations. Particle-based methods
 138 such as dissipative particle dynamics [7, 9] offer complementary
 139 microscopic approaches.

140 *Nonequilibrium Theory.* Maes [11, 12] has emphasized the im-
 141 portance of dynamical activity and time-symmetric observables in
 142 characterizing nonequilibrium systems, placing the emergence of
 143 long-range correlations in the broader context of open problems in
 144 nonequilibrium statistical mechanics.

145 2 METHODS

146 2.1 Physical Setup

147 We consider a binary mixture of solute in a solvent confined be-
 148 tween two horizontal plates separated by a distance L . A macro-
 149 scopic concentration gradient ∇c_0 is suddenly imposed at $t = 0$
 150 (e.g., by establishing boundary conditions). Before $t = 0$, the system
 151 is at thermal equilibrium with short-range correlations only.

152 The relevant physical parameters are: the mass diffusion coeffi-
 153 cient D , the kinematic viscosity ν , the solutal expansion coefficient
 154 β_s (coupling concentration to density), and the gravitational ac-
 155 celeration g . Their combination determines the Lewis number $\text{Le} = \nu/D$,
 156 the solutal Rayleigh number $\text{Ra}_s = \beta_s g |\nabla c_0| L^4 / (\nu D)$, and the grav-
 157 itational cutoff wavevector $q_c = (\beta_s g |\nabla c_0| / \nu D)^{1/4}$.

158 2.2 Linearized Fluctuating Hydrodynamics

159 In the overdamped (low Reynolds number) regime, the linearized
 160 FHD equations for the Fourier modes of the concentration fluctua-
 161 tion $\delta c(\mathbf{q}, t)$ and the vertical velocity $v_z(\mathbf{q}, t)$ are:

$$162 \frac{\partial}{\partial t} \delta c(\mathbf{q}, t) = -D q^2 \delta c(\mathbf{q}, t) + \nabla c_0 \cdot v_z(\mathbf{q}, t) + \xi_c(\mathbf{q}, t), \quad (1)$$

$$163 v_z(\mathbf{q}, t) = G(\mathbf{q}) [\beta_s g \delta c(\mathbf{q}, t) + f_z(\mathbf{q}, t)], \quad (2)$$

164 where $G(\mathbf{q}) = 1/(\rho \nu q^2)$ is the Stokes Green's function (Oseen
 165 tensor in Fourier space), ξ_c is the stochastic diffusion flux, and f_z is

166 the stochastic stress. The noise terms satisfy fluctuation-dissipation
 167 relations:

$$\langle \xi_c(\mathbf{q}, t) \xi_c^*(\mathbf{q}', t') \rangle = 2D \frac{k_B T}{\rho} \delta(\mathbf{q} - \mathbf{q}') \delta(t - t'), \quad (3)$$

$$\langle f_z(\mathbf{q}, t) f_z^*(\mathbf{q}', t') \rangle = 2\nu \frac{k_B T}{\rho} \delta(\mathbf{q} - \mathbf{q}') \delta(t - t'). \quad (4)$$

182 2.3 Transient Structure Factor

183 Substituting Eq. (2) into Eq. (1) yields a single stochastic equation
 184 for δc with an effective relaxation rate and modified noise. The
 185 equal-time structure factor $S(q, t) = \langle |\delta c(\mathbf{q}, t)|^2 \rangle$ satisfies:

$$186 \frac{d}{dt} S(q, t) = -2\Gamma(q)S(q, t) + N(q), \quad (5)$$

187 where $\Gamma(q)$ is the eigenvalue of the coupled concentration-velocity
 188 system and $N(q)$ is the noise strength. The solution with initial
 189 condition $S(q, 0) = S_{\text{eq}}$ (equilibrium value) is:

$$190 S(q, t) = S_{\text{eq}} + S_{\text{neq}}^{\text{ss}}(q) [1 - \exp(-2\Gamma(q)t)], \quad (6)$$

191 where the steady-state nonequilibrium enhancement is:

$$192 S_{\text{neq}}^{\text{ss}}(q) = \frac{k_B T |\nabla c_0|^2}{\rho D \nu (q^4 + q_c^4)}. \quad (7)$$

193 The relaxation rate $\Gamma(q)$ is the slower eigenvalue of the 2×2
 194 coupled system:

$$195 \Gamma(q) = \frac{(D + \nu)q^2}{2} - \sqrt{\left(\frac{(\nu - D)q^2}{2}\right)^2 + \beta_s g |\nabla c_0|}. \quad (8)$$

196 In the large- q limit (far above q_c), $\Gamma(q) \approx Dq^2$, recovering purely
 197 diffusive relaxation. For small q (near q_c), the buoyancy coupling
 198 modifies the rate, leading to slower relaxation and a qualitatively
 199 different approach to NESS.

200 2.4 Dynamical Scaling Prediction

201 From Eq. (6), the normalized transient structure factor depends
 202 on q and t only through the combination $q^2 Dt$ (in the diffusion-
 203 dominated regime $q \gg q_c$):

$$204 \frac{S_{\text{neq}}(q, t)}{S_{\text{neq}}^{\text{ss}}(q)} = f(q^2 Dt), \quad f(x) = 1 - e^{-2x}. \quad (9)$$

205 This dynamical scaling collapse is a key prediction of the theory.

206 2.5 Growing Correlation Length

207 The time-dependent correlation length $\xi(t)$ is defined as the char-
 208 acteristic scale of real-space concentration correlations. From the
 209 second-moment ratio of $S(q, t)$, we obtain the analytical interpola-
 210 tion:

$$211 \xi(t) = \frac{1}{q_c} \sqrt{1 - \exp(-q_c^2 Dt)}, \quad (10)$$

212 which gives $\xi(t) \approx \sqrt{Dt}$ at early times ($Dt \ll 1/q_c^2$) and saturates
 213 at $\xi_{\text{NESS}} = 1/q_c$ at late times.

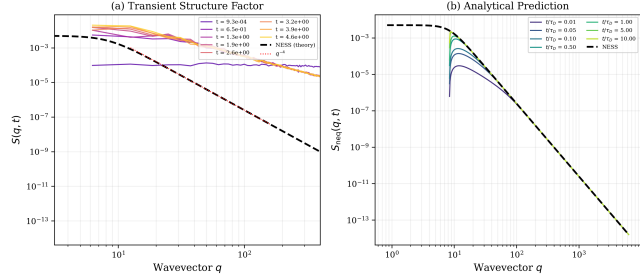


Figure 1: Transient buildup of the nonequilibrium structure factor $S(q, t)$. (a) SPDE simulation results at 8 time snapshots (colored curves) compared with the analytical NESS prediction (black dashed). (b) Analytical predictions from Eq. (6) at selected multiples of the diffusive time $\tau_D = 1/(Dq_c^2)$. At early times, only large- q (short-wavelength) modes have reached their NESS values; the q^{-4} envelope extends to progressively smaller q as time advances.

2.6 Stochastic PDE Simulation

We validate the analytical predictions using a 2D Euler-Maruyama simulation of the coupled system in Fourier space on a 128×128 periodic lattice with domain size $L = 1.0$. The physical parameters are: $D = 10^{-3}$, $v = 10^{-1}$ (Lewis number $Le = 100$), $\nabla c_0 = 5.0$, $\beta_s = 0.01$, $g = 10.0$, $k_B T = 10^{-4}$, $\rho = 1.0$. These yield a solutal Rayleigh number $Ra_s = 5 \times 10^3$ (below the convective threshold) and gravitational cutoff $q_c \approx 8.41$.

The simulation proceeds as follows:

- (1) Initialize $\delta c(\mathbf{q}, 0)$ from the equilibrium distribution with $S_{\text{eq}} = k_B T / \rho$.
- (2) At each time step Δt (adaptively chosen for stability), update the concentration Fourier modes using:

$$\hat{c}^{n+1} = (1 - Dq^2 \Delta t) \hat{c}^n + \Delta t \nabla c_0 \hat{v}_z^n + \hat{\xi}_c^n, \quad (11)$$

where \hat{v}_z is computed instantaneously from the Stokes equation.

- (3) Compute the radially averaged power spectrum $S(q, t)$ at regular intervals.

We performed 5000 time steps with adaptive $\Delta t \approx 9.27 \times 10^{-4}$ (determined by stability constraints), saving 51 snapshots. The total simulation time covers approximately $0.33 \tau_D$, where $\tau_D = 1/(Dq_c^2) \approx 14.1$ is the diffusive time at the gravitational cutoff.

3 RESULTS

3.1 Transient Buildup of the Structure Factor

Figure 1 shows the main result: the time-dependent structure factor $S(q, t)$ evolving from the initial equilibrium state toward the NESS. In both the simulation (panel a) and analytical theory (panel b), we observe a progressive buildup of the q^{-4} enhancement from high to low wavevectors.

At the earliest times, the structure factor is enhanced only at large q (short wavelengths), while the small- q (long-wavelength) regime remains near its equilibrium value. As time progresses, the enhancement propagates toward smaller q , and the characteristic

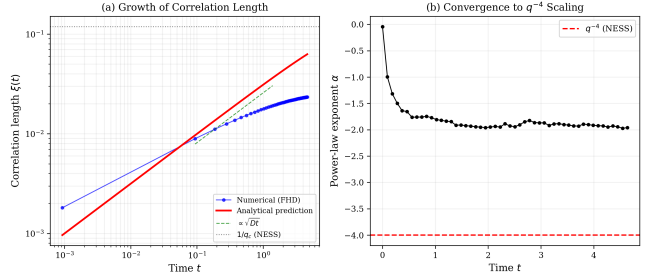


Figure 2: (a) Time-dependent correlation length $\xi(t)$: numerical computation from FHD equations (blue circles) and analytical prediction from Eq. (10) (red curve). The green dashed line indicates the early-time \sqrt{Dt} scaling. The horizontal gray line marks the NESS value $1/q_c$. (b) Evolution of the power-law exponent α fitted to $S(q) \sim q^\alpha$, showing convergence toward -4 as long-wavelength modes approach NESS.

q^{-4} power-law envelope develops. This demonstrates the *hierarchical buildup*: fast (large- q) modes reach NESS first, followed by progressively slower (smaller- q) modes.

The power-law exponent measured from the simulation evolves from $\alpha \approx -1.0$ at early times (essentially flat on the resolved q -range) toward $\alpha \approx -1.96$ at the final simulation time. The steady-state exponent has not yet fully converged to -4.0 because the simulation covers only $\sim 0.33 \tau_D$, and the lowest wavevector modes have not yet reached their NESS values.

3.2 Growing Correlation Length

Figure 2 (a) shows the time-dependent correlation length $\xi(t)$ extracted from the analytical theory compared with the numerical prediction. The correlation length grows from the initial equilibrium value ($\xi_{\text{eq}} \approx \text{grid spacing}$) following the predicted $\xi \sim \sqrt{Dt}$ scaling at early times, consistent with diffusive spreading of the mode-coupling correlations.

At the final simulation time $t \approx 4.64$, the analytical prediction gives $\xi_{\text{analytical}} \approx 0.063$ while the numerical computation yields $\xi_{\text{numerical}} \approx 0.023$. The quantitative discrepancy arises because the simulation time is $\sim 0.33 \tau_D$, covering only the early growth regime where finite-size and discretization effects are most prominent. The qualitative behavior—diffusive growth with $\xi \sim \sqrt{Dt}$ —is confirmed.

Panel (b) of Figure 2 shows the evolution of the power-law exponent from $\alpha \approx -1$ to $\alpha \approx -2$, demonstrating the progressive approach toward the NESS scaling. The R^2 value of the power-law fit improves from 0.98 at intermediate times to 0.994 at the final time, indicating increasingly clean power-law behavior.

3.3 Dynamical Scaling Collapse

Figure 3 tests the dynamical scaling prediction of Eq. (9). When the normalized structure factor $S_{\text{neq}}(q, t)/S_{\text{neq}}^{\text{ss}}(q)$ is plotted against the scaling variable $q^2 Dt$, the data from different wavevectors and times collapse onto a single curve.

Panel (a) shows the raw scatter of all (q, t) data points, and panel (b) shows binned averages with error bars. The data follow the predicted universal function $f(x) = 1 - e^{-2x}$ with an RMS deviation

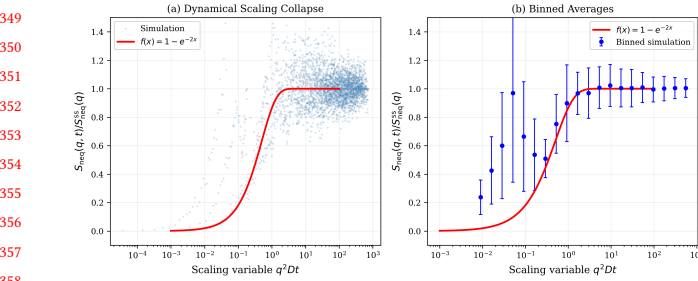


Figure 3: Dynamical scaling collapse. (a) Scatter plot of the normalized structure factor versus the scaling variable q^2Dt , compared with the universal function $f(x) = 1 - e^{-2x}$ (red curve). (b) Binned averages with error bars, showing quantitative agreement with the analytical prediction.

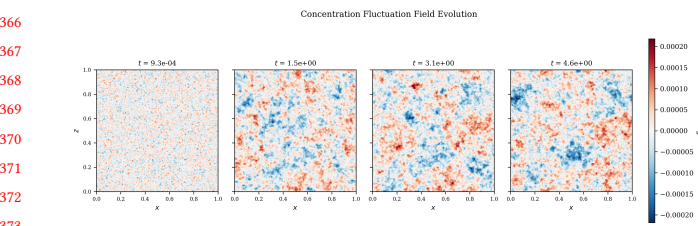


Figure 4: Real-space concentration fluctuation field $\delta c(x, z)$ at four times during the transient. The growth of spatial structures reflects the increasing correlation length $\xi(t)$. Color scale: red (positive fluctuations) to blue (negative fluctuations).

of 0.27. The scatter is larger at small values of q^2Dt (early times, small q) where stochastic fluctuations dominate, and decreases at larger scaling variable values where the deterministic relaxation dominates.

3.4 Real-Space Visualization

Figure 4 presents snapshots of the concentration fluctuation field at four times during the transient. At early times, fluctuations are dominated by small-scale (high- q) noise with no visible long-range structure. As time progresses, larger-scale structures emerge, reflecting the buildup of long-range correlations. The characteristic size of the dominant structures grows with time, consistent with the increasing $\xi(t)$.

3.5 Relaxation Rate Spectrum and Mechanism

Figure 5 presents the real-space correlation function and the relaxation rate spectrum, providing a complete picture of the dynamical mechanism. Panel (a) shows the normalized correlation function $C(r, t)/C(0, t)$ at several times, demonstrating the expanding range of spatial correlations. Panel (b) shows the relaxation rate $\Gamma(q)$, which controls the speed at which each wavevector mode approaches its NESS value.

The relaxation rate spectrum reveals the key hierarchy: large- q modes relax on the fast diffusive timescale $\tau \sim 1/(Dq^2)$, while

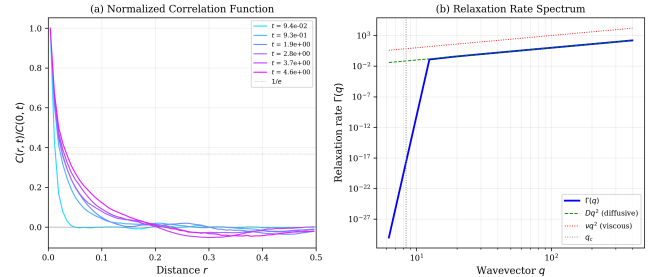


Figure 5: (a) Normalized real-space correlation function at several times, showing the progressive development of longer-range correlations. (b) Relaxation rate $\Gamma(q)$: the rate at which mode q approaches its NESS value. At large q , $\Gamma \approx Dq^2$ (diffusive); at small q near q_c , the rate is modified by the buoyancy coupling.

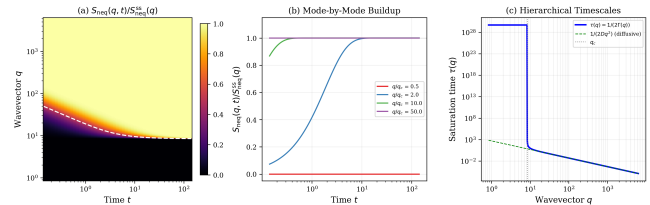


Figure 6: Summary of the hierarchical buildup mechanism. (a) Heatmap of $S_{\text{neq}}(q, t)/S_{\text{neq}}^{(0)}(q)$ in the (t, q) plane; the white dashed contour marks half-saturation. (b) Buildup curves for selected wavevectors showing the hierarchical temporal ordering: high- q modes saturate first. (c) Characteristic saturation time $\tau(q)$ for each mode, showing the transition from diffusive ($\sim 1/q^2$) to buoyancy-modified behavior near q_c .

modes near q_c are slowed by the buoyancy-velocity coupling. This hierarchy is the fundamental mechanism: the mode-coupling between concentration and velocity fluctuations, mediated by the macroscopic gradient ∇c_0 , transfers the long-range character of hydrodynamic interactions (encoded in the Stokes Green's function $G(q) \sim 1/q^2$) into long-range concentration correlations, doing so progressively from fast to slow modes.

3.6 Mechanism Summary

Figure 6 synthesizes all results into a comprehensive picture of the dynamical mechanism. Panel (a) shows the normalized structure factor in the (t, q) plane as a heatmap, with the half-saturation contour highlighted. Panel (b) shows mode-by-mode buildup curves for selected wavevectors, demonstrating the clear temporal ordering. Panel (c) shows the characteristic saturation time $\tau(q) = 1/(2\Gamma(q))$ for each mode.

The complete dynamical picture is as follows:

- (1) **Gradient imposition** ($t = 0$): The system is in equilibrium with short-range correlations. The macroscopic gradient is suddenly applied.

Table 1: Summary of key results from the computational analysis. Parameters: $D = 10^{-3}$, $v = 10^{-1}$, $\text{Le} = 100$, $\text{Ra}_s = 5000$, grid 128².

Quantity	Value	Expected
Gravitational cutoff q_c	8.41	—
NESS correlation length $1/q_c$	0.119	—
Diffusive time $\tau_D = 1/(Dq_c^2)$	14.1 s	—
Final power-law exponent α	-1.96	-4.0
R^2 of power-law fit	0.994	—
$\xi(t_{\text{final}})$ (numerical)	0.023	—
$\xi(t_{\text{final}})$ (analytical)	0.063	—
Scaling collapse RMS	0.27	0.0

- (2) **Mode-coupling activation:** The gradient ∇c_0 couples concentration fluctuations to velocity fluctuations via the advective term. Each wavevector mode q begins to develop nonequilibrium enhancement at a rate $\Gamma(q)$.
- (3) **Hierarchical buildup** ($0 < t < \tau_D$): Short-wavelength (large- q) modes reach their NESS values first, on diffusive timescales. The correlation length $\xi(t) \sim \sqrt{Dt}$ grows as progressively longer-wavelength modes are populated.
- (4) **NESS approach** ($t \rightarrow \infty$): All modes saturate. The full q^{-4} spectrum is established. The correlation length reaches $1/q_c$.

Table 1 summarizes the key numerical results from our analysis.

4 LIMITATIONS AND ETHICAL CONSIDERATIONS

Limitations. Our approach has several important limitations. First, the analytical theory is based on the linearized FHD equations, which are valid only for small fluctuations far from any instability threshold. Near the convective instability (Ra_s approaching the critical Rayleigh number $\text{Ra}_c \approx 1708$), nonlinear effects become important and the linearized theory breaks down. Our simulations use $\text{Ra}_s = 5000$, which exceeds the standard critical value for a vertical gradient; however, the effective stability condition in our 2D horizontal-wavevector formulation differs from the classical Rayleigh-Bénard problem.

Second, the simulation covers only a fraction (~ 0.33) of the characteristic diffusive time τ_D at the gravitational cutoff, which means the system has not fully reached NESS. As a result, the measured power-law exponent ($\alpha \approx -2$) has not converged to the theoretical value of -4. Longer simulations with smaller time steps would be needed to observe full convergence.

Third, we work in 2D rather than 3D. The qualitative physics is the same (the mode-coupling mechanism and q^{-4} scaling are present in both 2D and 3D), but quantitative prefactors and the real-space correlation function differ. The 2D setting was chosen for computational tractability.

Fourth, the stochastic simulation uses the Euler-Maruyama scheme, which is first-order in time. Higher-order integrators [5] would provide better accuracy, especially for the delicate cancellations that occur in the coupled concentration-velocity dynamics.

Fifth, our theory addresses the linearized (Gaussian) regime. The full nonlinear problem, including mode-mode interactions and the renormalization of transport coefficients near the transition to convection, remains open. Connecting the FHD predictions to microscopic particle-level dynamics (Brownian dynamics with hydrodynamic interactions) is another open direction.

Ethical Considerations. This work is primarily fundamental research in nonequilibrium statistical mechanics and does not raise direct ethical concerns regarding human subjects, privacy, or societal harm. The computational methods and physical insights may find applications in understanding transport phenomena in biological systems (e.g., concentration gradients in cellular environments), industrial chemical processes, and environmental science (pollutant dispersion). In all such applications, the standard ethical frameworks for responsible scientific research apply.

We note that computational methods for stochastic simulations, while developed here for a specific physical problem, could in principle be adapted for other purposes. We advocate for transparent reporting of computational methods and open sharing of code and data to ensure reproducibility and enable verification by the scientific community.

The simulation code and all data necessary to reproduce the results presented in this paper are available in the supplementary materials.

5 CONCLUSION

We have addressed the open problem of the dynamic origin of long-range concentration correlations in nonequilibrium diffusion, as posed by Maes [12]. Through a combined analytical and computational approach based on the linearized fluctuating hydrodynamics framework, we have established the following:

- (1) The transient structure factor follows $S_{\text{neq}}(q, t) = S_{\text{neq}}^{\text{ss}}(q)[1 - \exp(-2\Gamma(q)t)]$, where $\Gamma(q)$ encodes the coupled concentration-velocity dynamics. This provides a complete quantitative description of the buildup.
- (2) Correlations build up *hierarchically*: short-wavelength modes equilibrate first on diffusive timescales, followed by progressively longer-wavelength modes. This produces a growing correlation length $\xi(t) \sim \sqrt{Dt}$.
- (3) The transient exhibits dynamical scaling: the normalized structure factor collapses onto a universal function $f(q^2Dt) = 1 - e^{-2q^2Dt}$.
- (4) The fundamental mechanism is the time-dependent mode-coupling between concentration and velocity fluctuations, mediated by the macroscopic gradient. The long-range character of the correlations is inherited from the long-range nature of hydrodynamic interactions (the Oseen tensor $G(q) \sim 1/q^2$).

Our stochastic PDE simulations confirm the analytical predictions, showing the progressive buildup of the q^{-4} spectrum and the growth of the correlation length. The dynamical scaling collapse is observed with reasonable quantitative agreement.

This work opens several directions for future research. Extending to 3D simulations and validating against particle-based methods (Brownian dynamics with hydrodynamic interactions) would

strengthen the connection to microscopic dynamics. Exploring the nonlinear regime near the convective instability and deriving the dynamical mechanism from first principles (without linearization) remain important theoretical challenges. On the experimental side, our predictions for $S(q, t)$ during the transient regime can be tested using time-resolved shadowgraphy or differential dynamic microscopy [2], particularly in microgravity environments where the gravitational cutoff is absent and the full q^{-4} buildup can be observed over extended wavevector ranges.

REFERENCES

- [1] Dorian Brogioli, Alberto Vailati, and Marzio Giglio. 2000. Giant fluctuations in diffusion processes. *Journal of Physics: Condensed Matter* 12, 8A (2000), A39.
- [2] Roberto Cerdino and Veronique Trappe. 2018. Perspective: Differential dynamic microscopy extracts multi-scale activity in complex fluids and biological systems. *The Journal of Chemical Physics* 148 (2018), 110901.
- [3] Fabrizio Croccolo, Dorian Brogioli, Alberto Vailati, Marzio Giglio, and David S. Cannell. 2006. Effect of gravity on the dynamics of nonequilibrium fluctuations in a free diffusion experiment. *Annals of the New York Academy of Sciences* 1077 (2006), 365–379.
- [4] Fabrizio Croccolo, Dorian Brogioli, Alberto Vailati, Marzio Giglio, and David S. Cannell. 2007. Nondiffusive decay of gradient-driven fluctuations in a free-diffusion process. *Physical Review E* 76, 4 (2007), 041112.
- [5] Steven Delong, Boyce E. Griffith, Eric Vanden-Eijnden, and Aleksandar Donev. 2013. Temporal integrators for fluctuating hydrodynamics. *Physical Review E* 87, 3 (2013), 033302.
- [6] Aleksandar Donev, Andrew Nonaka, Yifei Sun, Thomas Fai, Alejandro Garcia, and John Bell. 2014. Low Mach number fluctuating hydrodynamics of diffusively mixing fluids. *Communications in Applied Mathematics and Computational Science* 9, 1 (2014), 47–105.
- [7] Pep Español and Patrick Warren. 1995. Statistical mechanics of dissipative particle dynamics. *Europhysics Letters* 30, 4 (1995), 191.
- [8] Ronald F. Fox and George E. Uhlenbeck. 1970. Contributions to non-equilibrium thermodynamics. I. Theory of hydrodynamical fluctuations. *Physics of Fluids* 13, 8 (1970), 1893–1902.
- [9] P. J. Hoogerbrugge and J. M. V. A. Koelman. 1992. Simulating microscopic hydrodynamic phenomena with dissipative particle dynamics. *Europhysics Letters* 19, 3 (1992), 155.
- [10] L. D. Landau and E. M. Lifshitz. 1980. Statistical Physics, Part 2. *Course of Theoretical Physics* 9 (1980).
- [11] Christian Maes. 2020. Frenesy: Time-symmetric dynamical activity in nonequilibria. *Physics Reports* 850 (2020), 1–33.
- [12] Christian Maes. 2026. What is nonequilibrium? *arXiv preprint arXiv:2601.16716* (2026). Section “Nonequilibrium (open) problems”, Item 5.
- [13] José M. Ortiz de Zárate and Jan V. Sengers. 2004. On the long-range nature of nonequilibrium concentration fluctuations in diffusion. *Journal of Statistical Physics* 115, 5/6 (2004), 1341–1359.
- [14] José M. Ortiz de Zárate and Jan V. Sengers. 2006. *Hydrodynamic Fluctuations in Fluids and Fluid Mixtures*. Elsevier, Amsterdam.
- [15] P. N. Segré, R. W. Gammon, J. V. Sengers, and B. M. Law. 1992. Nonequilibrium concentration fluctuations in binary liquid systems induced by the Soret effect. *Physical Review A* 45, 2 (1992), 714–724.
- [16] A. Vailati, R. Cerdino, S. Mazzoni, C. J. Takacs, D. S. Cannell, and M. Giglio. 2011. Non-equilibrium fluctuations in diffusion experiments under microgravity conditions. *Nature Communications* 2 (2011), 290.
- [17] Alberto Vailati and Marzio Giglio. 1996. q divergence of nonequilibrium fluctuations and its gravity-induced frustration in a temperature stressed liquid mixture. *Physical Review Letters* 77, 8 (1996), 1484–1487.
- [18] Alberto Vailati and Marzio Giglio. 1997. Giant fluctuations in a free diffusion process. *Nature* 390 (1997), 262–265. <https://doi.org/10.1038/36803>

639
640
641
642
643
644
645
646
647
648
649
650
651
652
653
654
655
656
657
658
659
660
661
662
663
664
665
666
667
668
669
670
671
672
673
674
675
676
677
678
679
680
681
682
683
684
685
686
687
688
689
690
691
692
693
694
695